

Infrared emission towards SN 1987A, 11 years after outburst: Properties of the circumstellar dust

Jg. Fischera, R. J. Tuffs, and H. J. Völk

Max-Planck-Institut für Kernphysik, Saupfercheckweg 1, 69115 Heidelberg, Germany

Received 30 April 2002 / Accepted 28 August 2002

Abstract. Detailed models are presented for the late epoch mid infrared (MIR) emission from collisionally heated grains in the shocked circumstellar gas around SN 1987A. Thermal dust emission from a region of moderate density interior to the thick inner ring seen with the Hubble Space Telescope (HST) is found to be a natural explanation for the MIR spectral energy distribution measured by ISOCAM. The MIR-spectrum can be reproduced by a mixture of silicate-iron or silicate-graphite grains or by a composition of pure graphite grains. A composition of pure iron grains on the other hand can be excluded and a pure silicate composition does not seem to be very likely. The dust-to-gas ratio in the interaction zone is $\sim 0.01\%$, an order of magnitude lower than estimates for dust abundances in the winds of red supergiant (RSG) stars in the LMC. This low dust abundance can be accounted for by a combination of evaporation through the UV-flash from the supernova outburst and subsequent sputtering in the shocked gas. For this explanation to hold, dust in the pre-supernova circumstellar medium (CSM) would have to have been predominantly composed of grains other than graphite, with a maximum size smaller than $\sim 0.1 \mu\text{m}$.

Key words. stars: supernovae: individual: SN 1987A – infrared: ISM – stars: circumstellar matter

1. Introduction

SN 1987A, a supernova of Type II, made it possible for the first time to make detailed observations of the interaction of a supernova ejecta with the very innermost region of its CSM. IR measurements enable us to analyse the abundance, composition, and size distribution of the circumstellar dust grains and to study grain destruction processes such as evaporation by the UV-flash of the supernova outburst and sputtering in the shocked gas behind a very strong shock. From this, new insights into the history of the progenitor star can be obtained, providing a more complete picture of the SN 1987A.

SN 1987A is the first supernova for which the progenitor was observed prior to outburst. It has been identified as the most luminous star of the system Sanduleak $-69^{\circ}202$ in the Large Magellanic Cloud (LMC) (West 1987) which had been classified as a blue supergiant (BSG) of spectral Type B3 I (Rousseau 1978). Observations with the HST showed a complex axis symmetrical structure of its CSM with a thick inner ring with a diameter of $\sim 1''.6$ and two outer rings with larger diameter at each side seen with a viewing angle of $\sim 43^{\circ}$ (Burrows et al. 1995). The analysis of dust scattered light of the supernova outburst suggest that the rings are connected with gas and dust distributed in an hour glass – shaped shell (Crotts et al. 1995).

Initially, the supernova ejecta freely expanded in the thin wind of the BSG, driving a blast wave into the CSM with a velocity of $\sim 30\,000 \text{ km s}^{-1}$. The reappearance of the radio emission (Staveley-Smith et al. 1992) almost coincidentally with the appearance of soft X-ray emission detected by ROSAT (Beuermann et al. 1994; Gorenstein et al. 1994) indicated that after ~ 1200 days the blast wave had reached denser material interior to the thick inner ring, which slowed down the shock velocity to $2900 \pm 480 \text{ km s}^{-1}$ (Gaensler et al. 1997). Chevalier & Dwarkadas (1995) supposed that this denser gas is comprised of material from a RSG phase of the progenitor of SN 1987A before it evolved into the BSG that finally exploded. They referred to this region, in which the gas should be ionised through the photon flux of the progenitor star of SN 1987A, as the “HII-region”. The interaction between the fast thin wind of the BSG and the slow moving thick wind of a RSG is also thought to be responsible for the larger structure of the CSM (Blondin & Lundqvist 1993; Martin & Arnett 1995).

In a previous paper (Fischera et al. 2002, Paper I) we presented MIR measurements, made with ISOCAM (Cesarsky et al. 1996) towards SN 1987A 11 years after the outburst. These reveal the central region around the supernova position as a resolved MIR source with an extension and orientation consistent with the elliptical projection of the thick inner ring, suggesting that the MIR emission is mainly circumstellar in origin. We found this emission is most probably from dust, collisionally heated in the shocked gas downstream of the blast wave as it expanded into the material of the HII-region

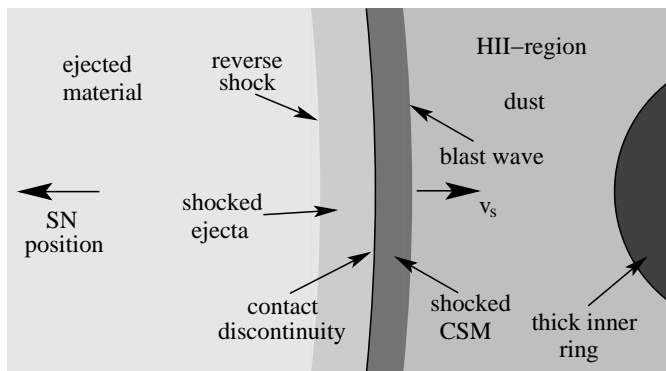


Fig. 1. Cartoon of the basic structure caused by the interaction of the expanding ejecta with the HII-region.

interior to the thick inner ring. On a purely energetical basis, all the emission could be from condensates in the metal rich core region of the expanding ejecta (Fischera 2000). However, as argued in Paper I, an emission which arises mainly from condensates does not explain the measured extension or orientation of the MIR source.

In this paper we present detailed calculations of emission from grains in the shocked CSM to analyse the implications of the ISOCAM measurements for the abundance, composition and size distribution of the circumstellar grains. In Sect. 2 we describe the dust model used to analyse the dust properties in the shocked CSM. Quantitative results are presented in Sect. 3. In Sect. 4 we discuss probably the most important destruction processes, which are evaporation of grains through the UV-flash and sputtering in the shocked gas downstream of the blast wave. In Sect. 5 this is used to derive information on grain abundance, and composition in the CSM prior to the supernova outburst. A summary is given in Sect. 6. As in Paper I we will assume a distance of 51 kpc to the supernova.

2. Modelling the MIR emission from the shocked CSM

We consider grains that are collisionally heated in the shocked circumstellar plasma downstream of the blast wave.

The structure caused by the interaction of the expanding ejecta with its CSM is visualised in Fig. 1. The shocked circumstellar gas is compressed to a thin layer that grows approximately as $0.1v_s t$ (Chevalier 1982), where v_s is the assumed constant speed of the blast wave and t the time since the shock reached the HII-region. Downstream it is bounded by the contact discontinuity to the shocked outer parts of the expanding ejecta. This ejected material is heated by both the reverse shock and by a shock reflected from the inner boundary of the HII-region (Borkowski et al. 1997). It is thought to be the origin of the strong emission in Ly α and H α at a distance of ~ 0.6 of the radius of the thick inner ring (Michael et al. 1998), that was measured by the HST close to the time of the ISOCAM observations. We do not expect strong MIR emission from the shocked ejected material for the following reasons:

1. The material at the reverse shock is mainly hydrogen and has such a low abundance in metals (e.g. Woosley 1988),

Table 1. Parameters of the shocked gas.

	model I	model II
shock velocity v_s	4100 km s ⁻¹	2900 km s ⁻¹
electron temperature T_e	2×10^7 K	2×10^7 K
ion temperature T_i	6×10^8 K	3×10^8 K
hydrogen density n_H	300 cm ⁻³	600 cm ⁻³
helium density n_{He}	$2.5 (n_{He})_\odot$	$2.5 (n_{He})_\odot$
metallicity Z	$0.3 Z_\odot$	$0.3 Z_\odot$

that, if any, only very few grains may have been formed in this region of the ejecta.

2. Further, as we show later (see Sect. 4), the grain charge and the strength of the magnetic field in the shocked CSM in the interaction zone makes it unlikely, that an observable amount of circumstellar grains have been overtaken by the outer parts of the ejecta.
3. The gas density of the ejecta at the reverse shock is, following the numerical results from Borkowski et al. (1997), much less than the density downstream of the blast wave. In consequence, the heating of any ejected grains at the reverse shock should be much weaker than for circumstellar grains downstream of the blast wave.

2.1. Gas parameters

The collisional heating of a grain in a hot plasma depends mainly on the temperatures of electrons and ions and the number density of the different species of the gas¹. We fix these properties to be broadly consistent with the observed radio and X-ray emission from the CSM. An analysis of the X-ray observations made with the ROSAT satellite towards SN 1987A up to and including the epoch of the ISOCAM observations is given in Appendix A. For temperatures above $\sim 10^7$ K, as encountered in the shocked gas, the grain heating of the smaller grains principally contributing to the emission observed by ISOCAM is mainly determined by the plasma density (see e.g. Dwek & Arendt 1992). As the physical conditions are somewhat uncertain we will consider two cases (models I and II) with different temperatures and densities. The parameters of models I and II are summarised in Table 1 and will be justified in the following.

Borkowski et al. (1997) have shown that an assumption of constant density, as suggested by Chevalier & Dwarkadas, can explain the soft X-ray emission (Hasinger et al. 1996) until at least 3000 days after outburst. They derived a pre-shock hydrogen density of 75 cm⁻³ with a corresponding shock speed v_s of the blast wave of 4100 km s⁻¹. In their calculations the HII-region was modelled as a thick torus in which the inner ring seen by the HST is embedded. They also mentioned that for a different structure of the HII-region higher densities would be possible. Indeed, a shock speed of 2900 ± 480 km s⁻¹ as derived from radio observations (Gaensler et al. 1997) would require a hydrogen density of the HII-region of about 150 cm⁻³.

¹ In general the heating, in particular the heating by the ions, has also a dependency on the relative motion of the grains in comparison to the motion of the gas, which is neglected for simplicity.

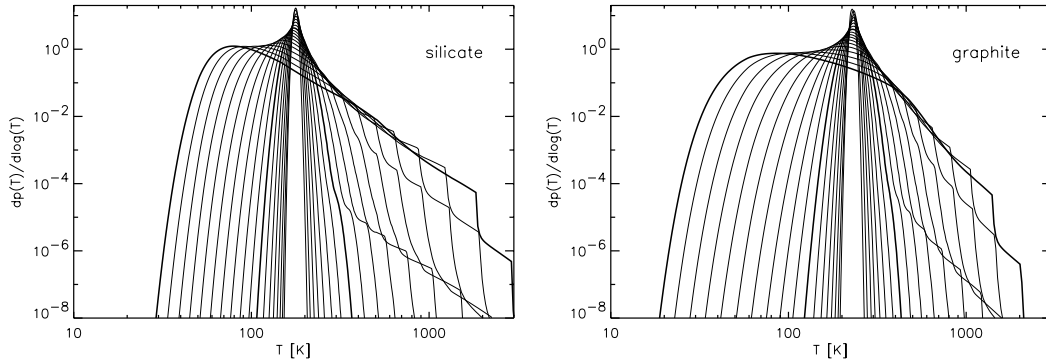


Fig. 2. Temperature distributions of spherical silicate and graphite grains for various grain sizes in the shocked CSM, assuming a density of the shocked gas of $n_{\text{H}} = 300 \text{ cm}^{-3}$ (model I). The variation in size between two lines is $d\log(a[\mu\text{m}]) = 0.1$. The temperature distributions, shown with thicker lines, belong to grains with a radius of $0.001 \mu\text{m}$ and $0.01 \mu\text{m}$. The steps in the $p(T)$ -curves are due to the approximation used for ion heating and appear roughly at temperatures where the thermal energy of the grains is equal to the threshold energy of the ions (see also Popescu et al. 2000).

It might also be possible, that the density increased with time (see Appendix A) although the X-ray measurements are also consistent with a constant external density.

For simplicity we assume that at the time of the ISOCAM observations the blast wave was still expanding into a homogeneous HII-region. We will consider hydrogen densities of 75 cm^{-3} (model I) and 150 cm^{-3} (model II) for the pre-shock region. The density of the gas is assumed to be compressed by a factor of four downstream of the blast wave and to stay constant in the whole interaction zone.

In converting the densities given by Borkowski et al. into hydrogen number density and ionic abundances needed for the calculation of dust heating (Sect. 2.2) we adopted the abundances of the thick inner ring given by Lundqvist & Fransson (1996). On this basis we took helium to be a factor of 2.5 more abundant than in the sun, and approximated the metallicity of all heavier elements to be 0.3 solar.

Because of the long equipartition time of the shocked circumstellar plasma the electron temperature should be much lower than the temperature for the ions and should increase with the distance to the outer shock (see e.g. Burrows et al. 2000). Thus, in calculating the grain heating we use two different temperatures for electrons and ions. As for the density, the temperature of the shocked CSM is taken to be independent of position.

The ion temperature T_{i} is taken to be (see e.g. Longair 1997)

$$T_{\text{i}} = 2 \frac{\gamma - 1}{(\gamma + 1)^2} \frac{\mu m_{\text{H}}}{k_{\text{B}}} v_{\text{S}}^2 \quad (1)$$

with $\gamma = 5/3$ and an atomic weight of $\mu = 1.6$ appropriate to the abundances in the CSM.

For the electrons we choose a temperature close to those derived from X-ray observations and predicted by numerical calculations appropriate to SN 1987A. From X-ray observations made with the ROSAT-satellite Hasinger et al. (1996) derived a temperature of approximately $T_{\text{e}} \approx 1.2 \times 10^7 \text{ K}$. Analysing the X-ray spectrum of SN 1987A, taken later with CHANDRA, using a shock model with a constant T_{e} , a higher electron temperature of the order of $\sim 3.5 \times 10^7 \text{ K}$ was found

(Burrows et al. 2000; Park et al. 2002). In our calculation we will adopt $T_{\text{e}} = 2 \times 10^7 \text{ K}$.

2.2. Calculation of the dust emission

The dust in the CSM is taken to be spherical for simplicity as there is no observational evidence for other grain shapes in the CSM of SN 1987A. Spherical grains are also generally assumed in the literature for grains produced in stellar winds (e.g. Gail & Sedlmayr 1999). However, if the grains are not too different from being spherical this assumption should not influence significantly our results about the properties of the grains in the CSM. For example, it has been found, that the temperature of spheroidal grains heated by the interstellar radiation field (ISRF) can only vary by more than 10% if the axial ratio exceeds a value of 2 (Voshchinnikov et al. 1999).

The grains are heated by collisions with electrons and ions of the hot ionized shocked plasma. The gas species is assumed to transfer all (if it sticks) or only a part (if it is not stopped) of the kinetic energy into thermal energy of the grain. The calculation of the energy deposition of non-stopping particles is based on their stopping-distances (ranges) in solids². For the heating by ions we considered in addition to hydrogen and helium also the next most abundant elements oxygen, nitrogen and carbon. The emission from larger grains we derived from their equilibrium temperatures. For smaller grains, where the deposited energy is typically larger than the thermal energy, we took their temperature fluctuations into account. The model for stochastic dust emission from a hot plasma is described in more detail in Popescu et al. (2000). As typical dust species we consider graphite and silicate grains. The temperature distributions of very small silicate and graphite grains in model I are shown in Fig. 2 where it can be seen, that small grains can be heated to very high temperatures. The smallest grains with 10 \AA radius will reach temperatures well above their

² The stopping power is due to ionisation losses in case of electrons. In case of the ions at energies considered here the stopping power is partly due to interaction with the electrons and partly due to inelastic scattering with the nucleons of the target material.

evaporation temperature. The grains contributing to the measured IR emission should therefore not be smaller than this size.

Because iron is expected to form in cool stellar outflows independent of the C/O ratio and is potentially one of the main condensates in the circumstellar environment of oxygen rich stars (see e.g. Gail & Sedlmayr 1999, and references there), we also carried out calculations for pure iron grains. For electrons in iron grains we used the analytical expression for the electron range in graphite derived by Dwek & Smith (1996) on basis of observational data, correcting for the different density. The optical properties of iron spheres we derived using MIE-theory (Bohren & Huffman 1983), whereby we included the dependence of the dielectric function in the IR on size and temperature of the iron grains (Fischera 2000). For the heat capacity of iron grains cooler than 298 K we used values tabulated in the American Institute of Physics Handbook (1972). For iron grains warmer than this we used an analytical expression for the heat capacity given by Chase (1998), assuming that iron is in the α - δ -phase.

2.2.1. Grain temperatures in the shocked CSM

The variation of the equilibrium temperature of spherical silicate, graphite, and iron grains in the shocked CSM is shown in Fig. 3. The different behaviour of the three species allows some information about dust composition to be derived from the ISOCAM measurements. Grain temperatures for the case $T_e = 3.5 \times 10^7$ K are also given. As seen in the figure the grain temperature of small silicate and graphite grains is nearly insensitive to T_e since the electrons are not stopped by the grains. The equilibrium temperatures are consistent with the colour temperatures T_c we derived in Paper I for a modified Planck spectrum $F_\lambda \propto \lambda^{-\beta} B_\lambda(T_c)$, where $B_\lambda(T_c)$ is the Planck function, ranging from ~ 200 K ($\beta = 2$) to ~ 290 K ($\beta = 0$). Because of stronger heating due to the higher grain density and the weaker cooling due to lower emissivities in comparison to silicate and graphite grains pure iron grains attain the highest temperatures. We also note that for the conditions in the shocked CSM, graphite grains are hotter than silicate grains. In less dense plasmas (e.g. $n_H = 1 \text{ cm}^{-3}$) one would expect a slightly higher temperature for silicate grains (Dwek 1987; Fischera 2000).

The temperature of small spherical iron grains depends strongly on grain size. This was also noted by Chlewicki & Laureijs (1988) for iron grains heated by the interstellar radiation field.

2.2.2. Grain size distribution in the CSM

In order to construct a SED for comparison with the data a functional form for the grain size distribution must be adopted. The size distribution of the grains in the shocked circumstellar environment of SN 1987A is not known and might be modified in comparison to the initial distribution in the CSM by different processes like evaporation during the UV-flash or sputtering in the shocked gas as will be shown later. However, for simplicity we assume, that the grains in the shocked CSM have a

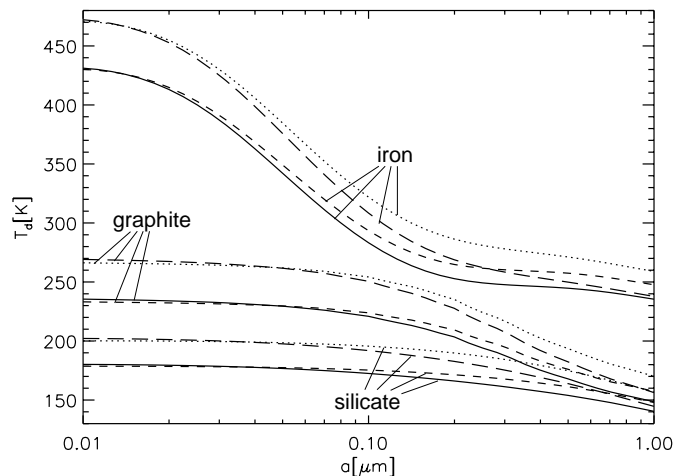


Fig. 3. Equilibrium temperatures of spherical silicate, graphite and iron grains as a function of grain radius a in the shocked gas downstream of the blast wave. The grain temperatures in models I and II are represented by the solid and the long dashed line, respectively. Also shown is the effect of raising T_e from 2×10^7 K to 3.5×10^7 K (short dashed and dotted lines, respectively, for models I and II).

grain size distribution similar to grains in the ISM of our galaxy and can be described by a simple power law $dn \propto a^{-k} da$ with power index k and a minimum and a maximum grain size a_{\min} and a_{\max} . Following Biermann & Harwit (1980) a power law distribution should be a general description of a grain size distribution resulting from grain-grain collisions and would especially describe the grain size distribution in the atmospheres of red-giants. In contrast to the emission from grains in the ISM, heated by the ISRF, where only stochastically heated small grains can achieve high enough temperatures to emit at shorter wavelengths (Draine & Anderson 1985), in the shocked CSM of SN 1987A larger grains can also contribute to the measured fluxes. The composite SEDs are relatively insensitive to a_{\min} , which we fixed at 10 \AA .

2.2.3. Free dust model parameters

For each of models I and model II for the shocked gas we made calculations taking various combinations of the following parameters as free variables:

- M_d , the dust mass. This was a scaling parameter in all calculations.
- k , the exponent in the grain size distribution $dn(a) \propto a^{-k} da$.
- a_{\max} , the maximum grain size.
- Grain composition. Five compositions were considered: Pure silicate, pure graphite, pure iron, a silicate-iron mixture and a silicate-graphite mixture. The relative composition in the mixtures was considered as a free variable.

The most probable values for the variables were found through a χ^2 -fit to the measured flux densities, taken from Paper I, which we colour corrected (see Blommaert et al. 2001) on the basis of the modelled spectrum. In addition we derived for each fit the luminosity L_d of the theoretical dust emission spectrum. The one sigma uncertainties of the parameters were calculated

from the χ^2 -fit by varying $\Delta\chi_1^2 = \chi_1^2 - \chi_{\min}^2$ until $\Delta\chi_1^2 = 1$ (see e.g. Press et al. 1992). To estimate the uncertainties of the fitted parameters a_{\min} , k and the dust mixture the dust mass M_d was taken to be a free variable. For simplicity the uncertainty of M_d itself was derived with all other parameters fixed.

3. Results

The results of the model calculations are summarised in Table 2, where we give for each fit also the reduced χ^2_ν , where ν is the number of free parameters. The best fits obtained for the two mixtures are shown in Fig. 4 together with the fitted spectrum for silicate grains. The emission spectrum is such that measurements at longer wavelengths (e.g. Lundqvist et al. 1999) are too insensitive to probe the emission from this region. The fits can be summarised as follows:

1. Fit parameter: M_d .

We simply compared the measured flux densities in the IR with the theoretical emission spectra of three different grain compositions (pure silicate, graphite or iron) with fixed grain size distribution for $a_{\max} = 0.25 \mu\text{m}$ and $k = 3.5$ as proposed for the grains in the ISM (MRN, 1977).

For both model I and model II a better fit is achieved under the assumption of pure graphite grains instead of silicate grains in the circumstellar environment. As seen in Fig. 4 the flux at $6.7 \mu\text{m}$ is too high to be emitted from silicate grains. Because of the high predicted temperatures a pure iron composition is even more unlikely.

2. Fit parameter: k , M_d .

For each of pure silicate, graphite and iron we varied the power k of the size distribution with fixed $a_{\max} = 0.25 \mu\text{m}$. The derived grain size distributions for graphite grains in model I and for silicate grains in both models are consistent with $k = 3.5$. For graphite grains in model II, which reach too high temperatures, a flatter distribution ($k < 2.25$) is required. No grain size distribution could be found which admitted a pure iron solution.

3. Fit parameter: Dust mixture, M_d .

For a fixed grain size distribution with power $k = 3.5$ and $a_{\max} = 0.25 \mu\text{m}$ we varied the composition of circumstellar grains, for a mixture of silicate with iron grains and a mixture of silicate with graphite grains.

Excellent fits could be achieved for silicate-iron mixture in model I and for the silicate-graphite mixture in model II (see also Fig. 4).

4. Fit parameter: a_{\max} , M_d .

For a given dust composition (silicate, graphite and the two derived mixtures) and a fixed size distribution with power $k = 3.5$ we varied a_{\max} .

The maximum grain sizes in model I are significantly smaller than in model II. In model I for silicate, graphite or the silicate-graphite mixture a better fit can be achieved with $a_{\max} < 0.25 \mu\text{m}$. The estimated maximum grain sizes of all considered compositions in model II are several times larger. We also examined a pure iron composition and found that the maximum grain size would be unrealistically large with $a > 10 \mu\text{m}$.

Due to the large number of free parameters several solutions with different compositions and grain size distributions are possible. The derived values like a_{\max} , k or the mixture of the composition are interrelated and depend on the plasma density. Despite these uncertainties the following conclusions could be reached largely independent of the assumptions:

1. Luminosity

For the luminosity of the collisionally heated dust 11 years after outburst we obtained (dependent on composition and the assumed plasma density) values for L_d in the range 2.91×10^{28} to 3.35×10^{28} W. This can be compared with the crude estimate of $L_d = 2.5 \times 10^{28}$ W given in Paper I where we approximated the dust emission spectrum with a simple modified black body spectrum. As already mentioned in Paper I the luminosity in the MIR is larger than in X-rays. Despite the increase of the X-ray luminosity since detection ~ 1400 days after outburst (Hasinger et al. 1996) the luminosity in the energy range 0.5 to 10 keV even ~ 13 years after outburst was only $L_X \approx 2 \times 10^{28}$ W (Burrows et al. 2000).

2. Composition

The dust is most likely a mixture of silicate with iron or silicate with graphite. Also pure graphite gives a reasonable fit. Pure silicate on the other hand seems to be unlikely and pure iron can be excluded.

3. Dust-to-gas ratio

Considering only cases where a_{\max} is not larger than $0.25 \mu\text{m}$ the dust mass is found to be nearly independent of composition and grain size distribution. The corresponding acceptable fits for model I ($n_H = 300 \text{ cm}^{-3}$) yield dust masses in the range $(0.9 \text{ to } 1.1) \times 10^{-6} M_\odot$ and those for model II ($n_H = 600 \text{ cm}^{-3}$) yield dust masses in the range $(0.45 \text{ to } 0.67) \times 10^{-6} M_\odot$.

Taking these values the dust-to-gas ratio is only mildly dependent on gas density as one would also expect. The mass of the X-ray emitting gas is given approximately by

$$M_{\text{gas}} \sim \frac{m_H EM}{n_H}, \quad (2)$$

where EM is the emission measure from X-ray observations and m_H the hydrogen mass. We have taken the emission measure from Hasinger et al. (1996) with $(1.4 \pm 0.4) \times 10^{57} \text{ cm}^{-3} \sim 2500$ days after outburst and extrapolated this result with $t^{2.06}$ (see Appendix A) to 4000 days. Using Eq. (2) we derive a gas mass of $1.0 \times 10^{-2}/n_H [300 \text{ cm}^{-3}] M_\odot$. Overall, this yields a dust-to-gas ratio in the range $(0.9 \text{ to } 1.3) \times 10^{-4}$.

If the grain size distribution is allowed to extend to grains with radii much larger than $0.25 \mu\text{m}$ the acceptable fits imply that the dust-to-gas ratio could be as high as 2.2×10^{-4} . As will be seen in Sect. 4 the pre-supernova dust abundance would however be almost unaffected.

4. Destruction processes due to the supernova

To compare the results for dust abundance and dust composition in the CSM of SN 1987A with expectations for the CSM

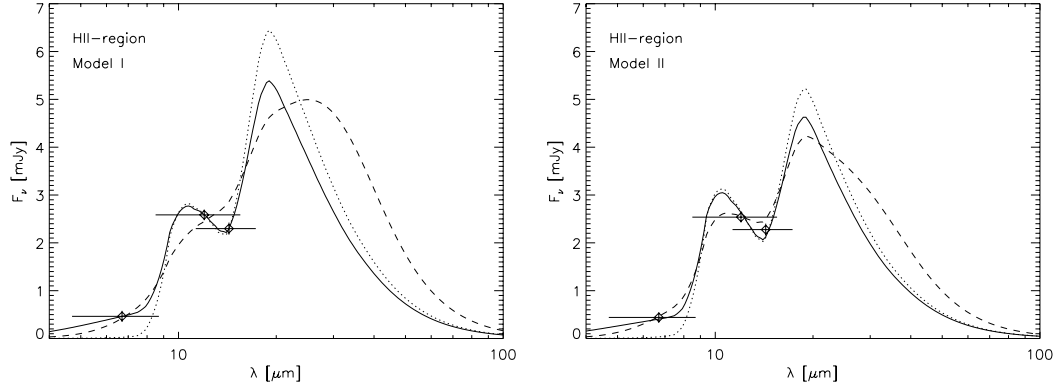


Fig. 4. Theoretical emission spectra of dust in the shocked circumstellar medium of SN 1987A for model I ($n_{\text{H}} = 300 \text{ cm}^{-3}$) and model II ($n_{\text{H}} = 600 \text{ cm}^{-3}$). Shown are spectra from pure silicate (dotted line) and the best fits with a mixture of silicate with graphite (dashed line) and with a mixture of silicate with iron (solid line). The grains are assumed to have a grain size distribution $dn \propto a^{-3.5} da$ with minimum and maximum grain radii of 10 \AA and $0.25 \mu\text{m}$. The ISOCAM fluxes (triangles), shown with the widths of the filters as horizontal lines, have been colour corrected to the spectrum of the silicate-iron mixture. The shown uncertainties are the absolute uncertainties in the integrated flux densities (taken from Table 2 of Paper I) which are 25% ($6.75 \mu\text{m}$), 4.3% ($12 \mu\text{m}$) and 5.5% ($14.3 \mu\text{m}$). These uncertainties are a combination of the systematic calibration uncertainties, which dominates at 12 and $14.3 \mu\text{m}$, and the random uncertainties.

Table 2. Results from the dust modelling.

		results model I ($n_{\text{H}} = 300 \text{ cm}^{-3}$)					results model II ($n_{\text{H}} = 600 \text{ cm}^{-3}$)					
compos.	mixture ^a	k	$a_{\text{max}}[\mu\text{m}]$	$M_{\text{d}}[10^{-6} M_{\odot}]$	$L_{\text{d}}[10^{28} \text{ W}]$	χ_{ν}^2	mixture	k	$a_{\text{max}}[\mu\text{m}]$	$M_{\text{d}}[10^{-6} M_{\odot}]$	$L_{\text{d}}[10^{28} \text{ W}]$	χ_{ν}^2
single variable: M_{d} ($\nu = 2$)												
silicate	–	3.5	0.25	0.97 ± 0.03^b	2.94	6.1	–	3.5	0.25	0.50 ± 0.02	2.63	5.3
graphite	–	3.5	0.25	1.04 ± 0.04	3.35	1.6	–	3.5	0.25	0.56 ± 0.02	3.15	3.5
iron	–	3.5	0.25	1.31 ± 0.05	3.35	55.	–	3.5	0.25	0.86 ± 0.03	3.65	81.
two variables: M_{d} and k ($\nu = 1$)												
silicate	–	$3.99^{+0.23}_{-0.24}$	0.25	0.85 ± 0.03	2.83	8.9	–	$3.39^{+0.44}_{-1.32}$	0.25	0.51 ± 0.02	2.64	11.
graphite	–	$3.56^{+0.30}_{-0.61}$	0.25	1.03 ± 0.04	3.36	3.1	–	$<2.25^c$	0.25	0.67 ± 0.02	3.03	1.3
iron	–	<0.53	0.25	1.51 ± 0.05	2.54	7.8	–	<0.28	0.25	1.09 ± 0.04	2.59	18.
two variables: M_{d} and dust mixture ($\nu = 1$)												
si.+iron	$2.09^{+1.09}_{-0.61}$	3.5	0.25	1.11 ± 0.04	3.18	0.0	$2.33^{+1.56}_{-0.73}$	3.5	0.25	0.60 ± 0.02	2.96	2.4
si.+iron	$2.90^{+1.57}_{-0.82}$	3.5	0.10	0.97 ± 0.03	3.18	0.3	$3.09^{+2.09}_{-0.95}$	3.5	0.10	0.51 ± 0.02	2.95	4.4
si.+iron	$3.35^{+1.89}_{-0.95}$	3.5	0.06	0.93 ± 0.03	3.19	0.75	$3.39^{+2.41}_{-1.05}$	3.5	0.06	0.48 ± 0.02	2.96	5.7
si.+gra.	$0.25^{+0.56}_{-0.25}$	3.5	0.25	1.03 ± 0.03	3.27	2.4	$0.73^{+0.73}_{-0.38}$	3.5	0.25	0.53 ± 0.02	2.94	0.2
si.+gra.	$0.43^{+0.64}_{-0.33}$	3.5	0.10	0.93 ± 0.03	3.22	1.07	$0.84^{+0.74}_{-0.40}$	3.5	0.10	0.47 ± 0.02	2.92	0.47
si.+gra.	$0.52^{+0.68}_{-0.34}$	3.5	0.06	0.89 ± 0.03	3.20	0.55	$0.88^{+0.75}_{-0.40}$	3.5	0.06	0.45 ± 0.02	2.91	1.45
two variables: M_{d} and a_{max} ($\nu = 1$)												
silicate	–	3.5	$0.03^{+0.07}_{-0.02}$	0.78 ± 0.03	2.78	9.3	–	3.5	$0.51^{+1.93}_{-0.41}$	0.60 ± 0.02	2.70	10.2
graphite	–	3.5	$0.19^{+0.30}_{-0.15}$	1.01 ± 0.03	3.36	3.1	–	3.5	$0.97^{+1.60}_{-0.44}$	0.75 ± 0.03	3.13	3.3
si.+iron	2.09	3.5	$0.26^{+0.53}_{-0.15}$	1.12 ± 0.04	3.18	0.0	2.33	3.5	$1.55^{+10.0}_{-1.24}$	1.08 ± 0.04	3.05	0.9
si.+gra.	0.25	3.5	$0.05^{+0.14}_{-0.03}$	0.90 ± 0.03	3.28	1.0	0.73	3.5	$0.42^{+0.71}_{-0.33}$	0.59 ± 0.02	2.95	0.05

^a Relative mass of silicate to iron or silicate to graphite, respectively.

^b The uncertainty of M_{d} was derived with all other parameters fixed.

^c The limit given for k corresponds to $\chi^2(k) - \chi^2(k=0) = 1$; here M_{d} , L_{d} and χ_{ν}^2 were calculated for $k=0$.

prior to the supernova event, account must be taken of the grain destruction processes due to the supernova and its remnant.

Before quantitatively discussing grain evaporation (Sect. 4.1) and grain sputtering (Sect. 4.2) we briefly demonstrate that the grains are dynamically coupled to the gas due to the betatron effect. For example the potential of a graphite

grain with $a = 0.1 \mu\text{m}$ at a temperature of $T_i = 3 \times 10^8 \text{ K}$ is more than 30 Volt (Draine & Salpeter 1979a). The Larmor radius of the grain is given by $R_L = m_{\text{gr}} v_{\text{gr}} / Q_{\text{gr}} B$, where m_{gr} is the mass of the grain, v_{gr} the relative velocity of the grain to the gas (initially $\frac{3}{4} v_S$), Q_{gr} the grain charge and B the magnetic field. For B we adopt the value for equipartion

between magnetic field and relativistic particles (Longair 1997), calculated from an extrapolation of the synchrotron emission after 1200 days (Gaensler et al. 1997). Assuming the radio emission to arise from the same volume as the X-ray emission (see Appendix A), this yields $B \sim 10^{-7}$ T, in agreement with the value found by Ball & Kirk (1992). Taking the shock velocity to be 2900 km s^{-1} , as derived from radio observations (Gaensler et al. 1997), the larmor radius R_L is then of the order of 2.1×10^{11} m, which is less than $\sim 10^{-4}$ of the diameter of the radio emission region. By comparison, the distance of the outer blast wave to the contact discontinuity increases with $\sim 0.1 v_s t$ (Chevalier 1982). Thus, the grains comoved with the gas after roughly one month.

To discuss the mass loss due to evaporation and sputtering we assumed, as in our earlier examination of the IR emission, that the grains in the CSM at the time of the supernova explosion had a grain size distribution with $k = 3.5$. Again we choose as minimum grain size $a_{\min} = 10 \text{ \AA}$.

4.1. Evaporation during the UV-flash

The evaporation of grains in the neighbourhood of a supernova in general has already been the subject of earlier examinations (e.g. Draine & Salpeter 1979b; Draine 1981; Pearce & Mayes 1986) and also has been discussed for silicate grains for the SN 1987A (Emmering & Chevalier 1989; Timmermann & Larson 1993). All considered the effect of evaporation for single grain sizes only. Here we are interested in the mass loss of grains with a certain size distribution in the shocked plasma behind the outer shock front. We use more recent theoretical results for the spectrum, duration and luminosity of the UV flash (Ensmann & Burrows 1992). Apart from silicate we also consider iron and graphite grains.

As a reasonable assumption, we only consider the evaporation of grains during this UV-flash, when the grains reached their highest temperatures. For the luminosity, temperature, and duration of the UV-flash we take the theoretical results of the model *500full1* from Ensmann & Burrows (1992). For our calculation, the spectrum is taken to be a simple black body spectrum with the given colour temperature from Ensmann & Burrows normalised to the luminosity.

To simplify the derivation of the mass loss of grains during the UV-flash, we neglect the effect of stochastic heating and assume that all grains are at their equilibrium temperatures. The evaporation of atoms from the surface of a grain with temperature T_d leads to a reduction in radius, that can be described by

$$\frac{da[\mu\text{m}]}{dt[\text{s}]} \sim \frac{1}{3} 10^{11} e^{-W(a)/k_B T_d(a)}, \quad (3)$$

where k_B is the Boltzmann constant and $W(a)$ the energy single atoms need to escape from the surface, which depends on the radius of the grain because of the surface tension of the grain. The coefficient is chosen to be close to the value given by Guhathakurta & Draine (1989) and Voit (1991) for graphite and silicate. The energies $W(a)$ for silicate and graphite are adopted from Guhathakurta & Draine. For iron we adopt

$$W(a) = (50\,000 - 22\,000 N(a)^{-1/3}) k_B, \quad (4)$$

where $N(a)$ is the number of atoms in the grain. Here we have chosen a bounding energy of the atoms close to $U = 4.29 \text{ eV}$, given in Gerthsen et al. (1989), and a surface tension of $\sigma = 1.8 \text{ J/m}^2$, given in Levêfre (1979).

The total reduction $a_{\text{ev}}(a, t)$ of a grain with an initial radius a during the UV-flash after a time t is found by integrating Eq. (3). If the final radius $\tilde{a}(a, t) = a - a_{\text{ev}}(a, t)$ is smaller than 3 \AA , the grain is assumed to have evaporated. The final grain size distribution of non evaporated grains assumed to have an initial size distribution $dn(a) = f(a) da = A a^{-3.5} da$ with constant A given by:

$$\begin{aligned} \tilde{f}(\tilde{a}) d\tilde{a} &= f(a(\tilde{a})) \frac{da}{d\tilde{a}} d\tilde{a} \\ &= A (\tilde{a} + a_{\text{ev}})^{-3.5} \left(1 - \frac{da_{\text{ev}}}{da}\right)^{-1} d\tilde{a}. \end{aligned} \quad (5)$$

The derived size distributions of silicate and graphite grains for different distances are shown in Fig. 5. As the evaporation is a surface effect, the fractional change in radius of grains at the same temperature is larger for smaller grains. Therefore the number of small grains decreases much more rapidly than the number of bigger grains. In addition, at the same distance to the supernova smaller grains are generally heated to higher temperatures. Due to the exponential dependence of Eq. (3) the evaporation of smaller grains is faster, which causes the maxima in the distribution functions.

How much silicate, iron and graphite dust might have survived the UV-flash in a certain distance to the supernova is shown in Fig. 6 for three different maximum grain sizes (0.25 , 0.1 and $0.06 \mu\text{m}$). It can be seen that silicate grains evaporate out to larger distances from the supernova than graphite grains. This is partly due to the higher bounding energy of graphite grains but mainly caused by the much higher temperatures the silicate grains attain in comparison with graphite grains. This is the opposite of the situation for collisionally heated dust in the CSM.

The grains most probably responsible for the measured infrared fluxes originated from between the original inner boundary of the HII-region and the position of the blast wave 4000 days after outburst. The mass loss of iron and silicate grains in this region is comparable and significant even for the largest considered grain size of $0.25 \mu\text{m}$. This changes at larger distances from the supernova, where evaporation of predominantly small iron grains becomes much stronger. For graphite grains evaporation is unimportant for the whole HII-region.

The radially integrated evaporated dust masses of silicate, graphite and iron grains corresponding to the shown curves is given in Table 3. In the integration it is assumed that the shock surface area is proportional to the square of the distance r of the blast wave to the position of the supernova. The differences in the derived values for the two models are due to the different shock velocities, that give slightly different positions of the inner boundary and the outer shock.

4.2. Sputtering in the shocked gas

Behind the blast wave grains undergo sputtering. This is thought to be one of the most important destruction processes

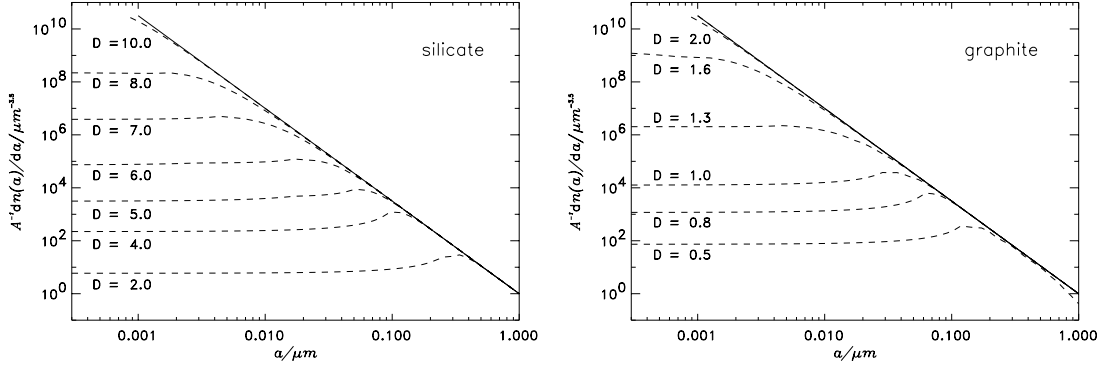


Fig. 5. Theoretical grain size distributions (dashed lines) of survived silicate and graphite grains after the UV-flash at various distances D (given in units of 10^{15} m) to the supernova. The initial size distribution is assumed to have been a power law $dn(a) = Aa^{-3.5} da$ with constant A (straight solid line).

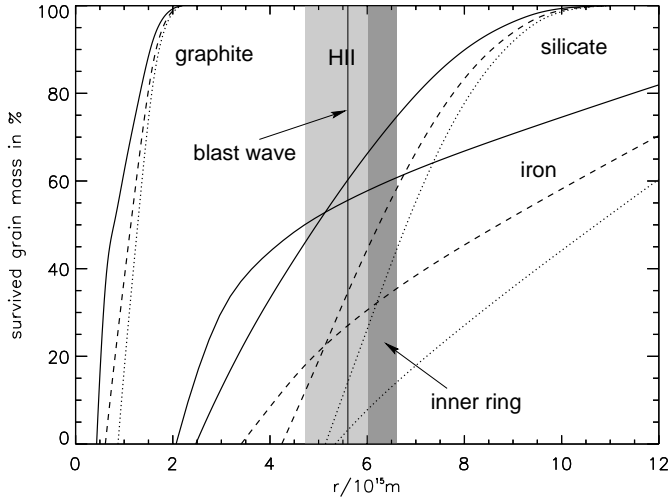


Fig. 6. Survived grain mass of graphite, silicate and iron grains after the UV-flash versus distance r from the supernova. It is assumed, that the grain size distribution before the supernova outburst had $k = 3.5$. a_{\min} is chosen to have been 10 \AA . The three curves (solid, dashed and dotted line) for each dust composition correspond to different choices for the initial maximum grain size a_{\max} (0.25, 0.1 and $0.06 \mu\text{m}$). Also shown is the approximate range of positions covered by the thick inner ring (dark grey) and the HII-region (light grey) before being caught by the blast wave. The inner radius of the HII-region was taken to be 4.72×10^{15} m. This was calculated from the observed position of the blast wave at epoch 3200 days (Gaensler et al. 1997) extrapolated to the epoch at which the shock first reached the HII-region (1200 days after outburst; Staveley-Smith et al. 1992). The vertical straight line at a radius of 5.43×10^{15} m indicates the position of the blast wave at the epoch of the ISOCAM observations (4000 days after outburst, also extrapolated from the observed position at 3200 days). The extrapolations were made assuming a velocity of 2900 km s^{-1} for the blast-wave corresponding to model II. If we take the velocity of 4100 km s^{-1} (model I) the inner boundary is closer to the supernova and the position of the blast wave further out.

in fast moving shocks (see e.g. Dwek et al. 1996). Sputtering time scales appropriate for a plasma with the abundances of the shocked CSM of SN 1987A are given in Appendix B.

Table 3. Mass loss through evaporation and sputtering.

$a_{\max} [\mu\text{m}]$	n_{H}^a	300 cm^{-3}			600 cm^{-3}		
		0.25	0.10	0.06	0.25	0.10	0.06
$\Delta M_{\text{sputt.}}^b$	sil.	27.7%	41.1%	50.3%	44.0%	61.7%	71.9%
$\Delta M_{\text{evap.}}$	sil.	49.4%	80.4%	98.3%	48.7%	79.2%	98.9%
$\Delta M_{\text{sputt.}}$	iron	27.2%	40.4%	49.5%	40.9%	58.1%	68.4%
$\Delta M_{\text{evap.}}$	iron	48.0%	78.6%	99.8%	47.7%	78.1%	100.0%
$\Delta M_{\text{total}}^c$	sil.	53.1%	82.4%	98.4%	58.4%	85.1%	99.1%
ΔM_{total}	iron	51.8%	81.0%	99.8%	56.4%	83.6%	100.0%
ΔM_{total}	gra. ^d	11.3%	17.3%	22.0%	19.1%	29.0%	36.3%

^a Density of the shocked gas downstream of the blast wave.

^b Sputtering without previous evaporation.

^c Mass loss after evaporation and following sputtering.

^d For graphite only the total mass loss is given because of an insignificant mass loss due to evaporation.

The final grain size distribution after a time Δt of an initial grain size distribution $f(a) da$ due to sputtering in a hot plasma is given by:

$$\tilde{f}(\tilde{a}, \Delta t) d\tilde{a} = f(a(\tilde{a}, \Delta t)) \frac{da}{d\tilde{a}} d\tilde{a} = f(\tilde{a} + \Delta a(\Delta t)) d\tilde{a}. \quad (6)$$

Because of the evaporation of grains during the UV-flash, the grain size distribution $f(a) da$ entering the sputtering zone is dependent on the distance to the supernova. The average grain size distribution at the time t after the shock reached the HII-region at time t_0 is therefore proportional to:

$$\langle \tilde{f}(\tilde{a}, t - t_0) \rangle \propto \int_{t_0}^t dt' v_S \tilde{f}(\tilde{a}, t - t', r(t')) r(t')^2, \quad (7)$$

where $t_0 = 1200$ days and the surface of the outer shock front is again assumed to increase with the square of the distance $r(t)$ of the blast wave to the supernova position.

The derived mass losses for the considered dust compositions and the three different maximum grain sizes are tabulated in Table 3. For comparison, we derived the sputtered dust mass with and without previous evaporation. The mass loss due to

Table 4. Solutions for dust in the pre-supernova CSM.

model	comp.	mixture ^a			10 ⁻⁴ M_d/M_{gas}		
		0.25 ^b	0.10	0.06	0.25	0.10	0.06
I	gra.	–	–	–	1.1	1.2	1.3
I	si.+iron	2.15	3.13	0.44	2.3	5.4	152
II	si.+iron	2.45	–	–	2.8	–	–
I	si.+gra.	0.47	2.02	25.4	1.4	2.4	20.
II	si.+gra.	1.42	4.01	62.3	1.8	3.6	48.

^a Relative mass of silicate to iron or silicate to graphite.

^b Maximum grain size in microns.

sputtering becomes progressively more important for the bigger grains. Whereas sputtering reduces the radius independent of the grain size, evaporation is the dominant destruction process for small grains. Graphite grains which are relatively stable against sputtering (Appendix B) and did not evaporate during the UV-flash (Sect. 4.1) suffer only moderate depletions compared to silicate and iron grains. In model I the initial mass of graphite grains would be less than a factor of 1.3 higher than that inferred from the ISOCAM observations for all considered maximum grain sizes.

5. Discussion

5.1. Dust in the pre supernova CSM

The modelling of the ISOCAM measurements (Sect. 3), combined with the calculations of grain destruction due to evaporation and sputtering (Sect. 4) allow us to infer grain abundances in the pre supernova CSM as well as to make crude estimates of maximum grain sizes and grain composition.

This information was derived for the best solutions ($\chi^2_\nu < 3$, Table 2) using the mass loss estimates given in Table 3 and is tabulated in Table 4. As expected the main parameter determining the composition and abundance of grains in the pre-supernova CSM is the maximum grain size. It is interesting to compare these quantities with observed and derived properties of circumstellar dust in stellar outflows.

We are not aware of direct measurements in the IR and submm regimes of dust abundances in the winds of LMC stars. We will simply estimate it by assuming that the dust abundance in the winds is proportional to the metallicity of the ISM. This is supported by Woods et al. (1992) who found that the outflow velocity of oxygen rich stars in the LMC is significantly lower than for oxygen rich stars in our galaxy and suggested that the lower velocity is due to the lower dust-to-gas ratio caused by the lower metallicity of the LMC. The same has also been proposed for high luminosity stars in the galactic anticentre which show only a modest outflow velocity (Habing et al. 1994). These works were confirmed by van Loon (2000), who found by comparing obscured Asymptotic Giant Branch stars of our galaxy, the Large and the Small Magellanic Clouds that the inferred dust-to-gas ratio of both carbon and oxygen rich stars is approximately proportional to the initial metallicity.

The winds of evolved carbon rich stars in our galaxy have generally been found to have dust-to-gas ratios in the range ~ 0.1 to $\sim 1\%$ (Jura 1986; Martin & Rogers 1987; Griffin 1990; Knapp et al. 1993; Bagnulo et al. 1995; and Olofsson et al. 1993; as quoted by Hiriart & Kwan 2000). On the other hand Hiriart & Kwan (2000) estimated from a subsample of Olofsson et al. a maximum dust-to-gas ratio of only $\sim 0.1\%$. For the galactic oxygen rich star OH 231.8+4.2, Knapp et al. (1993) obtained a dust abundance of $\sim 0.7\%$.

Scaling by the factor of 2 between the metallicity of the LMC and the metallicity of the solar vicinity (Russell & Dopita 1992) we would expect on this basis dust to gas ratios for LMC carbon stars in the range ~ 0.05 – 0.5% and for LMC oxygen stars of order $\sim 0.3\%$. Although clearly very uncertain, these numbers are nevertheless only consistent with a subset of the solutions of the pre-supernova gas-to-dust ratios in the CSM of SN 1987A given in Table 4. In particular, all the pure graphite solutions appear underabundant in dust by an order of magnitude compared with expectations for the winds of carbon stars. This confirms the expectation that the dust should in fact be silicate rich on the basis of the gas phase abundances in the inner ring (Lundqvist & Fransson 1996; Sonneborn et al. 1997).

The solutions for silicate-iron and silicate-graphite mixtures in Table 4 are consistent with the expected dust to gas ratios of $\sim 0.3\%$ for oxygen-rich stars provided the maximum grain size in the CSM of SN 1987A was smaller than $0.1 \mu\text{m}$. This is in accordance with findings, both theoretical and observational, that cool stars eject mainly small grains, irrespective of composition. An upper limit of $0.14 \mu\text{m}$ on the maximum sizes of grains around oxygen rich mass-losing stars was found by (Jura 1996). A maximum grain smaller than $\sim 0.1 \mu\text{m}$ is also consistent with the sizes found for the dust ejected from the carbon rich star IRC+10216 (Martin & Rogers 1987; Griffin 1990; Jura 1994; Bagnulo et al. 1995) or the typical sizes around evolved carbon stars derived by Hiriart & Kwan (2000).

On the other hand, this small maximum grain size contrasts with results for oxygen rich stars derived from their ultraviolet extinction. Rogers et al. (1983) suggested that the grains around μ Cep should be in the range $0.1 \mu\text{m}$ to $0.5 \mu\text{m}$. Based on extinction measurements made for α Sco, Seab & Snow (1989) concluded that the grains in the circumstellar environments of cool oxygen rich giants should be larger than $\sim 0.08 \mu\text{m}$ and possibly enrich the ISM with grains as large as $\sim 1 \mu\text{m}$. If this were also the case for the RSG wind of the progenitor of SN 1987A, the low dust abundance found by ISOCAM could neither be explained by evaporation nor by sputtering. It might then have had to have been intrinsically low. Alternatively, the grain abundance could have been reduced by radiation pressure (Turner & Pearce 1992) after the progenitor evolved to its final BSG phase 20 000 years ago (Crotts & Heathcote 1991). However for this, the coupling of the grains to the gas would have had to have been weak. Another scenario for reducing the grain abundance might be a mixing of the material of the BSG wind, with a negligible dust abundance, with that of the RSG wind at a dynamically unstable interface between the winds (García et al. 1996a, 1996b).

5.2. Iron abundance in the shocked CSM

On the basis of a spherically symmetrical hydrodynamical simulation of the interaction of the blast wave with the HII region, Borkowski et al. (1997) derived an upper limit on the gas phase iron abundance in the HII region of only 0.1 of the solar iron abundance from the X-ray spectrum measured with the ROSAT satellite (Hasinger et al. 1996). Comparing Chandra data with a plane parallel shock model Park et al. (2002) found a value of 0.07 of solar for the iron abundance in the X-ray emitting region between epochs 1999 and 2001. These gas phase abundances for iron are lower by a factor of at least ~ 3 compared to the iron abundance in the LMC from Russell & Dopita (1992), which is 36% of the solar abundance (determined from the photosphere; Anders & Grevesse 1989). This prompted Borkowski et al. to suppose that most of the iron was condensed into grains. However, this is not supported by the ISOCAM measurements. An upper limit for the mass of iron condensed in grains can be taken from the calculations for pure iron grains in the shocked CSM tabulated in Table 2. Taking for iron grain masses of $1.5 \times 10^{-6} M_{\odot}$ (model I) or $1.1 \times 10^{-6} M_{\odot}$ (model II) and the iron abundance in the LMC to be $n_{\text{Fe}}/n_{\text{H}} = 1.7 \times 10^{-5}$ (Russell & Dopita 1992), the fraction of iron in solid form is at maximum $\sim 32\%$ (model I) or $\sim 45\%$ (model II). For the better fitting silicate/iron mixtures the upper limits will be still lower. On the basis of this evidence, the HII-region would be underabundant in iron, whether in gaseous or condensed form. Further X-ray and infrared observations would be valuable to investigate this problem.

5.3. Outlook

In the short term, further observations to follow the MIR light curve will provide information on the dependence on radial position of the dust-to-gas ratios in the shocked HII region for comparison with model predictions. On the one hand there will be a tendency for the overall volume-averaged dust-to-gas ratios to be lowered due to sputtering at later epochs, if the upstream dust abundance is constant. On the other hand, the survived dust abundance after the UV-flash will increase with radius, especially for silicate and iron grains. Another potential reason for increasing dust abundances with radius could be a flushing out of grains from the inner regions of the CSM through radiation pressure, after the RSG turned into a BSG. This might also offer an explanation for the puzzle of the low iron abundance in both grains and gas inferred from the ISOCAM and ROSAT and CHANDRA data, as discussed above. As already stated this may require a weak coupling of the grains to the gas.

Observations of the brightening so-called “hot spots” seen in the optical (Lawrence et al. 2000) show that the blast wave is already interacting at certain places with dense material of the thick inner ring. The origin of the thick inner ring, is unknown. It is also not clear whether the MIR echo seen after 580 days (Roche et al. 1993) can be attributed to the ring. If the ring is composed of material from the red supergiant phase of the progenitor star (see e.g. Fransson et al. 1989), then one might anticipate a rapid increase in MIR luminosity with time, which would soon dominate the continuum emission from the

HII-region. The higher gas densities in the ring might lead to an accompanying increase in grain temperature, which would allow thermal dust emission from the thick inner ring to be distinguished from an increasing contribution from the HII region. If, on the other hand, the thick inner ring is composed of material from the companion star in the putative binary system (e.g. Podsiadlowski 1992) then one might speculate that the dust abundance and composition of the ring might deviate markedly from that of the HII region discussed in this paper.

6. Summary

The IR emission was analysed in terms of thermal emission from dust, collisionally heated by the shocked gas behind the blast wave that is expanding into the HII-region interior to the thick inner ring. We used a realistic grain model with a grain size distribution $dn \propto a^{-k} da$ including stochastically heating of small grains. For the shocked gas we considered two different models corresponding to the downstream densities $n_{\text{H}} = 300 \text{ cm}^{-3}$ (model I) and $n_{\text{H}} = 600 \text{ cm}^{-3}$ (model II). The conclusions for the shocked CSM are as follows:

1. The luminosity of the dust emission is found to range from 2.91 to $3.35 \times 10^{28} \text{ W}$ (according to assumed grain composition and plasma density).
2. The dust is most likely composed either of a silicate-iron or a silicate-graphite mixture or of pure graphite.
3. Considering only cases with a maximum grain size not larger than $0.25 \mu\text{m}$ the dust masses are, independent of the assumed grain composition and size distribution, $(0.9$ to $1.1) \times 10^{-6} M_{\odot}$ (model I) and $(0.45$ to $0.67) \times 10^{-6} M_{\odot}$ (model II). This corresponds for a gas mass of $1.0 \times 10^{-2}/n_{\text{H}}[300 \text{ cm}^{-3}] M_{\odot}$ to dust-to-gas ratios in the range $(0.9$ to $1.3) \times 10^{-4}$. For larger maximum grain sizes a larger range of the dust-to-gas ratio of up to 2.2×10^{-4} are admitted by the data.
4. For the LMC abundances of Russell & Dopita (1992) the maximum fraction of iron condensed into grains in the shocked CSM is 32% (model I) or 45% (model II).

We have calculated the grain destruction due to the UV-flash of the supernova outburst and subsequent sputtering downstream of the blast wave. From this we have deduced dust properties in the CSM prior to the supernova. Our conclusions are:

1. Pure graphite solutions for the pre-supernova CSM are underabundant in dust by an order of magnitude compared with estimates for the abundance of carbon grains in the winds of LMC-carbon stars.
2. Solutions for silicate-iron and silicate-graphite mixtures in the pre-supernova CSM are consistent with the expected dust-to-gas ratios of $\sim 0.3\%$ in the winds of oxygen rich LMC stars provided the maximum grain size was less than $\sim 0.1 \mu\text{m}$.

Acknowledgements. The work was supported by Deutsches Zentrum für Luft- und Raumfahrt e.V. (DLR) through the projects “50 OR 9702” and “50 OR 99140”. We have made use of the ROSAT Data Archive of the Max-Planck-Institut für extraterrestrische Physik (MPE) at Garching, Germany. We like to thank the referee Dr. S. Colgan for his helpful suggestions.

Table A.1. Derived rates of X-ray photons towards SN 1987A.

obs. time	day	instr. ^a	t_{int}/s	$N/1000\text{ s}$
12.02.91–13.02.91	1448	HRI (1)	23107	0.17 ± 0.90
06.10.91–07.10.91	1685	PSPCB	16398	2.72 ± 0.63
30.04.92–14.05.92	1898	PSPCB	9340	2.05 ± 0.76
04.12.92–06.12.92	2110	PSPCB	2552	5.12 ± 1.80
07.04.93–10.04.93	2235	PSPCB	11259	2.63 ± 0.73
20.06.93–05.07.93	2315	PSPCB	10391	3.13 ± 0.76
28.09.93–30.09.93	2409	PSPCB	9131	3.79 ± 0.85
20.06.94–20.09.94	2718	HRI (4)	12223	5.01 ± 1.62
03.10.94–02.01.95	2823	HRI (2)	18756	3.54 ± 0.91
01.04.95–11.07.95	3008	HRI (3)	28833	4.61 ± 0.97
10.10.95–10.01.96	3196	HRI (2)	26034	7.29 ± 1.15
16.04.96–31.07.96	3392	HRI (2)	46907	7.54 ± 0.89
22.10.96–12.01.97	3568	HRI (2)	45192	7.22 ± 0.87
21.02.97–02.03.97	3654	PSPCB	15440	8.31 ± 0.86
04.03.97–03.06.97	3706	HRI (2)	52601	8.31 ± 0.86
16.12.97–17.12.97	3948	HRI (1)	21738	12.6 ± 1.5
19.02.98–22.02.98	4014	PSPCB	19382	9.19 ± 0.78

^a Number in brackets give the number of observations used.

Appendix A: X-ray flux until 4000 days after outburst

Measurement of the X-ray flux from the SN 1987A until ~3000 days after outburst with the X-ray satellite ROSAT (Hasinger et al. 1996) showed a monotonic increase of the luminosity, where the variation in time could be linear or also steeper with $\propto t^{1.67 \pm 0.35}$. A linear trend would be consistent with a constant external density (Hasinger et al. 1996). Later measurements with CHANDRA ~13 years after outburst gave fluxes clearly above a linear trend (Burrows et al. 2000). To see how the X-ray flux evolved until the ISOCAM observations we derived the X-ray fluxes from a large number of available measurements that were made with the HRI and the PSPC instrument of ROSAT until ~4000 days after outburst. For a direct comparison with the data published by Hasinger et al. we also included measurements which were made before ~3000 days after outburst. The data were automatically calibrated with SASS. In calculating the counts of X-ray photons we used the same apertures to determine the source and the background counts used by Hasinger et al. (1996) and scaled the photon fluxes derived from the HRI-data with a factor 2.65 to allow comparison with the PSPC-data. To estimate the uncertainties we assumed poisson statistics for the source counts and gaussian statistics for the background noise.

The derived final counting rates of the observations are summarised in Table A.1 and shown in Fig. A.1 as open symbols. Until 3000 days after outburst they are consistent with the counting rates published by Hasinger et al. which are shown as black solid symbols. At later times the fluxes lay slightly above the linear trend. Fitting a potential to the counting rates derived here gives with a $\chi^2_{\text{min}} = 1.29$ a monotonic increase of:

$$N(t) \propto t^{2.06 \pm 0.20}. \quad (\text{A.1})$$

This may be because the shock is reaching denser material in time. On the other hand, numerical calculations for a

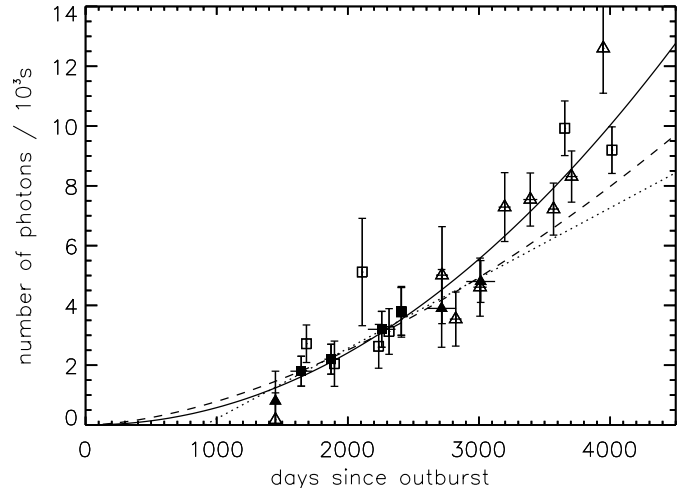


Fig. A.1. Time evolution of the X-ray emission of SN 1987A, measured with the ROSAT satellite. The photon fluxes derived from observations with the HRI and the PSPC instrument are shown as triangles and squares. Published data (filled symbols) until 3000 days after outburst (Hasinger et al. 1996) are shown for comparison. These data can be described through a linear increase (dotted line) since 900 days and a potential (broken line) with $\propto t^{1.67}$ (Hasinger et al. 1996). The photon fluxes derived here (open symbols) give an increase with $\propto t^{2.06 \pm 0.20}$ (solid line).

HII-region with homogeneous density do not give a linear trend of the X-ray luminosity for the first several years (Borkowski et al. 1997).

To derive the volume V of the X-ray emitting gas at the time of the ISOCAM observations ~4000 days after outburst we assumed that the X-ray luminosity was proportional to the emission measure $EM = n_e n_i V$, where n_e and n_i are the number density of the electrons and the ions. Taking the emission measure after ~2500 days to be $(1.4 \pm 0.4) \times 10^{57} \text{ cm}^{-3}$ (Hasinger et al. 1996; Borkowski et al. 1997) and the abundances as given in Sect. 2.1, this volume was approximately $2.2 \times 10^{52} \text{ cm}^3$.

Appendix B: Sputtering time scales for the shocked CSM

Here we derive sputtering rates specific to the physical conditions and abundances encountered in the shocked HII region around SN 1987A. At the high temperatures involved, sputtering is independent of grain charge and nearly independent of the plasma temperature. Sputtering reduces the radius of all grains of a given composition in a time Δt by the same amount $\Delta a(\Delta t)$. To derive the life times of the grains due to sputtering we used the formula (Eq. (27)) given by Draine & Salpeter (1979a) for non rotating grains moving with a relative velocity v_{gr} with respect to the gas with a temperature T_i . Sputtering yields were adopted from Tielens et al. (1994), and we considered sputtering due to H, He, C, N and O, adopting plasma abundances as given in Sect. 2.1. The initial relative velocities of grains overtaken by the blast wave ($v_{\text{gr}} = \frac{3}{4}v_s$) are so high that at first the sputtering is almost non thermal. Due to the drag forces the sputtering becomes thermal after some time, which increases the sputtering yield slightly (10%–30%). Here

we simply take the average of the sputtering yield of the two limits $v_{gr} = 0$ and $v_{gr} = 3v_s/4$. The resulting life times of the considered grains are:

$$\tau = \frac{a[0.01 \mu\text{m}]}{n_H[\text{cm}^{-3}]} \times \begin{cases} 11.5 \times 10^3 & \text{graphite} \\ 2.3 \times 10^3 & \text{silicate} \\ 2.7 \times 10^3 & \text{iron} \end{cases} \text{ years} \quad (\text{B.1})$$

in model I and

$$\tau = \frac{a[0.01 \mu\text{m}]}{n_H[\text{cm}^{-3}]} \times \begin{cases} 12.8 \times 10^3 & \text{graphite} \\ 2.9 \times 10^3 & \text{silicate} \\ 3.0 \times 10^3 & \text{iron} \end{cases} \text{ years} \quad (\text{B.2})$$

in model II.

References

- Anders, E., & Grevesse, N. 1989, *Geochim. Cosmochim. Acta*, 53, 197
- American Institute of Physics Handbook, 3 edition, 1972 (McGraw-Hill Book Company)
- Bagnulo, S., Doyle, J. G., & Griffin, I. P. 1995, *A&A*, 301, 501
- Ball, L., & Kirk, J. G. 1992, *ApJ*, 396, L39
- Beuermann, K., Brandt, S., & Pietsch, W. 1994, *A&A*, 281, L45
- Biermann, P., & Harwit, M. 1980, *ApJ*, 241, L105
- Blommaert, J., Siebenmorgen, R., Coulais, A., et al. 2001, *The ISO Handbook*, vol. III
- Blondin, J. M., & Lundqvist, P. 1993, *ApJ*, 405, 337
- Bohren, C. F., & Huffman, D. R. 1983, *Absorption and Scattering of Light by Small Particles* (John Wiley & Sons)
- Borkowski, K. J., Blondin, J. M., & McCray, R. 1997, *ApJ*, 476, L31
- Burrows, C. J., Krist, J., Hester, J. J., et al. 1995, *ApJ*, 452, 680
- Burrows, D. N., Michael, E., Hwang, U., et al. 2000, *ApJ*, 543, L149
- Cesarsky, C. J., Abergel, A., Agnese, P., et al. 1996, *A&A*, 315, L32
- Chase, M. W., Jr. 1989, *J. Phys. Chem. Ref. Data*, Monograph, 9, 1-1951
- Chevalier, R. A. 1982, *ApJ*, 258, 790
- Chevalier, R. A., & Dwarkadas, V. V. 1995, *ApJ*, 452, L45
- Chlewicki, G., & Laureijs, R. J. 1988, *A&A*, 207, L11
- Crotts, A. P. S., & Heathcote, S. R. 1991, *Nature*, 350, 683
- Crotts, A. P. S., Kunkel, W. E., & Heathcote, S. R. 1995, *ApJ*, 438, 724
- Draine, B. T., & Salpeter, E. E. 1979a, *ApJ*, 231, 77
- Draine, B. T., & Salpeter, E. E. 1979b, *ApJ*, 231, 438
- Draine, B. T. 1981, *ApJ*, 245, 880
- Draine, B. T., & Anderson, N. 1985, *ApJ*, 292, 494
- Dwek, E. 1987, *ApJ*, 322, 812
- Dwek, E., Foster, S. M., & Vancura, O. 1996, *ApJ*, 457, 244
- Dwek, E., & Smith, R. K. 1996, *ApJ*, 459, 686
- Hiriart, D., & Kwan, J. 2000, *ApJ*, 532, 1006
- Emmering, R. T., & Chevalier, R. A. 1989, *ApJ*, 338, 388
- Ensman, L., & Burrows, A. 1992, *ApJ*, 393, 742
- Fischera, Jg. 2000, *Infrarotemission der SN 1987A nach 11 Jahren*, Thesis, Heidelberg
- Fischera, Jg., Tuffs, R. J., & Völk, H. J. 2002, *A&A*, 386, 517 (Paper I)
- Fransson, C., Cassatella, A., Gilmozzi, R., et al. 1989, *ApJ*, 336, 429
- Gail, H.-P., & Sedlmayr, E. 1999, *A&A*, 347, 594
- Gaensler, B. M., Manchester, R. N., Staveley-Smith, L., et al. 1997, *ApJ*, 479, 845
- García-Segura, G., Mac Low, M.-M., & Langer, N. 1996, *A&A*, 305, 229
- García-Segura, G., Langer, N., & Mac Low, M.-M. 1996, *A&A*, 316, 133
- Gerthsen, C., Kneser, H. O., & Vogel, H. 1989, *Physik, Ein Lehrbuch zum Gebrauch neben Vorlesungen* (Springer-Verlag)
- Gorenstein, P., Hughes, J. P., & Tucker, W. H. 1994, *ApJ*, 420, L25
- Griffin, I. P. 1990, *MNRAS*, 247, 591
- Guhathakurta, P., & Draine, B. T. 1989, *ApJ*, 345, 230
- Habing, H. J., Tignon, J., & Tielens, A. G. G. M. 1994, *A&A*, 286, 523
- Hasinger, G., Aschenbach, B., & Trümper, J. 1996, *A&A*, 312, L9
- Jura, M. 1986, *ApJ*, 303, 327
- Jura, M. 1994, *ApJ*, 434, 713
- Jura, M. 1996, *ApJ*, 472, 806
- Knapp, G. R., Sandell, G., & Robson, E. I. 1993, *ApJS*, 88, 173
- Lawrence, S. S., Sugerman, B. E., Bouchet, P., et al. 2000, *ApJ*, 537, L123
- Lefèvre, J. 1979, *A&A*, 72, 61
- van Loon, J. Th. 2000, *A&A*, 354, 125
- Longair, M. S. 1997, *High Energy Astrophysics*, vol. 2 (Cambridge)
- Lundqvist, P., & Fransson, C. 1996, *ApJ*, 464, 924
- Lundqvist, P., Sollermann, J., Kozma, C., et al. 1999, *A&A*, 347, 500
- Martin, P. G., & Rogers, C. 1987, *ApJ*, 322, 374
- Martin, C. M., & Arnett, D. 1995, *ApJ*, 447, 378
- Mathis, J. S., Ruml, W., & Nordsieck, K. H. 1977, *ApJ*, 217, 425, (MRN)
- Michael, E., McCray, R., Pun, C. S. J., et al. 1998, *ApJ*, 509, L117
- Olofsson, H., Eriksson, K., Gustafsson, B., & Carlström, U. 1993, *ApJS*, 87, 267
- Park, S., Burrows, D. N., Garmire, G. P., et al. 2002, *ApJ*, 567, 314
- Seab, C. G., & Mayes, A. J. 1986, *A&A*, 155, 291
- Popescu, C. C., Tuffs, R. J., Fischera, Jg., & Völk, H. J. 2000, *A&A*, 354, 480
- Podsiadlowski, P. 1992, *PASP*, 104, 717
- Press, W. H., Teukolsky, S. A., Vetterling, W. T., & Flannery, B. P. 1992, *Numerical Recipes in C* (Cambridge)
- Roche, P. F., Aitken, D. K., & Smith, C. H. 1993, *MNRAS*, 261, 522
- Rogers, C., Martin, P. G., & Crabtree, D. R. 1983, *ApJ*, 272, 175
- Rousseau, J., Martin, N., Prévot, L., et al. 1978, *A&AS*, 31, 243
- Russell, S. C., & Dopita, M. A. 1992, *ApJ*, 384, 508
- Seab, C. G., & Snow, T. P. 1989, *ApJ*, 347, 479
- Sonneborn, G., Fransson, C., Lundqvist, P., et al. 1997, *ApJ*, 477, 848
- Staveley-Smith, L., Manchester, R. N., Kesteven, M. J., et al. 1992, *Nature*, 355, 147
- Tielens, A. G. G. M., McKee, C. F., Seab, C. G., & Hollenbach, D. J. 1994, *ApJ*, 431, 321
- Timmermann, R., & Larson, H. P. 1993, *ApJ*, 415, 820
- Turner, K., & Pearce, G. 1992, *Ap&SS*, 190, 1
- Voit, G. M. 1991, *ApJ*, 379, 122
- Voshchinnikov, N. V., Semenov, D. A., & Henning, Th. 1999, *A&A*, 349, L25-L28
- West, R. M., Laubert, A., Jørgensen, H. E., & Schuster, H.-E. 1987, *A&A*, 177, L1
- Wood, P. R., Whiteoak, J. B., Hughes, S. M. G., et al. 1992, *ApJ*, 397, 552
- Woosley, S. E. 1988, *ApJ*, 330, 218